Anomalous Behavior of the Equatorial Ionization Anomaly During the 2 July 2019 Solar Eclipse

O. F. Jonah[1] [ID]**, L. Goncharenko[1]** [ID]**, P. J. Erickson[1], S. Zhang[1]** [ID]**, A. Coster[1], J. L. Chau[2]** [ID]**, E. R. de Paula[3], and W. Rideout[1]**

[1]Haystack Observatory, Massachusetts Institute of Technology, Westford, MA, USA, [2]Leibniz Institute for Atmospheric Physics, Kühlungsborn, Germany, [3]National Institute for Space Research (INPE), Sao Jose dos Campos, Brazil

Abstract A solar eclipse is a spectacular phenomenon resulting from a Sun-Moon alignment as viewed from the Earth. Eclipses have a great influence on the state of the ionosphere and trigger significant variations during this extraordinary event, as daytime sunlight turns to darkness and back again. Therefore, understanding how this dramatic solar-lunar event affects the Earth's atmosphere is of enormous importance. In this study, we took advantage of the proximity of a 2 July 2019 solar eclipse to the equatorial ionization anomaly (EIA) in order to investigate EIA dynamics during the eclipse total obscuration as it made its first landfall over the South American continent. We found the following eclipse dynamic features (1) analogous to prior results at the EIA, a 57% enhancement of the total electron content (TEC) in the EIA crest during total obscuration in areas a few degrees to the north from totality; (2) a 35% TEC suppression along the path of totality to the south of the EIA (sub-EIA) crest; (3) temporal and spatial extension of the southern EIA crest; (4) enhancement of the fountain effect and associated with it vertical plasma drift in the magnetic equatorial region; and (5) unusual observation of TEC bite-out near the EIA crest prior to local eclipse onset.

1. Background

It is well-known that solar eclipses provide a special laboratory condition for researchers to study, substantiate, and quantify the effects associated with the estimated variation of solar radiation on a normal day compared to the "artificial" darkness caused by a total solar eclipse. This kind of study is important because the processes that control the ionosphere are extremely complex.

Solar eclipse influence on the variability of the whole ionosphere has been studied by many researchers (e.g., Coster et al., 2017; Goncharenko et al., 2018; Huba & Drob, 2017; Lin et al., 2018; Zhang et al., 2017). It is well established that during the short-lived solar eclipse, the whole ionosphere undergoes dramatic transformations. The energy from the Moon's shadow causes large suppression of electron density along the path of eclipse totality (Coster et al., 2017; Zhang et al., 2017) as well as enhancement at thousands of kilometers away from the eclipse totality (e.g., Chen et al., 2019; Goncharenko et al., 2018).

Solar eclipses at low and equatorial latitudes can induce especially complicated ionosphere and thermosphere changes. Cheng et al. (1992) investigated the ionospheric responses in the D, F1, and F2 layers to the solar eclipse of 23 September 1987 in locations close to the EIA crest region, using ionospheric vertical sounding data, VLF propagation delay data, and differential Doppler shift data. They found that the ionization in the ionosphere around the magnetic equator decreased at the onset of the solar eclipse and consequently caused ionization decrease at the EIA crest. After the maximum obscuration passed, the ionization at the magnetic equator started to increase (in response to the eclipse recovery with increasing solar irradiation), and as a result, more ionization was transported to low latitudes, triggering TEC increase at the EIA crest. Adeniyi et al. (2007) used ionogram parameters at an equatorial station over Ilorin, Nigeria (4.57°E, 8.53°N, dip 4.1°S) to document the effect of the 29 March 2006, solar eclipse. They showed that the electron density at true height was drastically decreased by 60% and 68% at the E and F1 layer, respectively, during the eclipse totality passage over Ilorin. Using data from 60 GPS TEC receivers over East Asia, Ding et al. (2010) studied the longest total eclipse of this century, which occurred on 22 July 2009. They observed a 5 TECu depletion caused by the eclipse and also found that ionospheric response to the solar eclipse is more intense at low latitudes in comparison with middle latitudes. (1 TECu $= 10^{16}$ electrons/m^2.)

However, Le et al. (2009) analyzed 21 solar eclipse events and pointed out that F2 peak electron density (NmF2) and TEC responses showed the same latitudinal dependence: The eclipse effects on NmF2 and TEC were smaller at low latitudes than at middle latitudes. The smaller NmF2 responses at low latitudes occurred mainly because of much higher heights of hmF2 at low latitudes and electron density response decreasing rapidly with increasing height.

A recent study by Zhang et al. (2017) showed the first unambiguous evidence of ionospheric bow waves in TEC along the totality path of the 21 August 2017 eclipse over the central United States. Using Millstone Hill observations, Goncharenko et al. (2018) further showed that midlatitude ionospheric response to the 2017 North America eclipse was dramatic even outside the totality region, causing a substantial 30–40% decrease in electron density and 100–220 K decrease in electron temperature. Coster et al. (2017) discussed the observation of large scale traveling ionospheric disturbances (LSTIDs) as another dynamic perturbation associated with eclipse totality. They observed strong suppression of LSTIDs in a region that moved with a speed comparable to the speed of the eclipse itself. Coster et al. (2017) also reported a 60% depletion of TEC along the eclipse totality path that exceeded all model predictions. Other eclipse studies using various iono-spheric sensors such as ground based incoherent scatter radars (Evans, 1965) and in situ observations from low earth-orbiting satellites (Tomás et al., 2007; Wang et al., 2010) have shown that the ionosphere electron density can be suppressed significantly as a consequence of the Moon's umbral and penumbral blockage of solar radiation during a total solar eclipse.

The response of the ionosphere to a solar eclipse may vary from middle latitudes to low latitudes mainly because of the different electrodynamic processes at the different regions, combined with significant differ-ences in the background thermosphere. For example, at middle latitudes, downward plasma diffusion and field-aligned transportation influence the electron distributions, whereas in equatorial and low-latitude regions, F region plasma is generally affected by the plasma drift in the vertical direction and by the field-aligned transportation. These latter competing effects influence the equatorial fountain effect, forming a trough at the magnetic equator and crests at $\pm15°$ of the magnetic equator. This plasma anomaly is known as the equatorial ionization anomaly (EIA). According to Chen et al. (2019), it is possible that atmospheric forcing due to neutral winds, originating from the large eclipse induced temperature gradient, causes an interaction with the magnetized conducting ionosphere in the E layer through reduced conductivity during the eclipse, and these effects perturb the $U \times B$ dynamo electric field. This enhanced electric field at ~10° latitude maps along highly conducting magnetic field lines to the equatorial F region height (at ~400 km) to produce the observed enhanced plasma fountain that is a primary control of the plasma density distribu-tion at the equatorial and low-latitude region. For these reasons, the case study of the 2 July 2019 eclipse described here represents a valuable opportunity to investigate the role of electrodynamics for the eclipse effects in the low-latitude ionosphere using a variety of modern-day observational tools.

As Rishbeth (1968) pointed out, eclipses each have a unique combination of spatial and temporal dynamic effects along with ionospheric and atmospheric preconditioning. Unlike the Great American total solar eclipse, which crossed the entire continental United States on 21 August 2017 and was the subject of studies referenced above, the total solar eclipse of 2 July 2019 traveled mostly over the Pacific Ocean, made its first continental landfall over the western side of South America at 20.44 UT (16.44 LT), and ended its journey at the eastern side of the continent at 21.55 UT (17.55 LT). This paper focuses on the effect of the 2 July 2019 solar eclipse over the EIA region and discusses the science behind observed anomalous changes of the eclipse-induced EIA crest. The unique feature of the present study is a significant TEC enhancement at the EIA crest throughout the eclipse period, along with the observation of simultaneous enhancement and depletion of ionization around the eclipse's total obscuration region.

2. Data and Methods

2.1. Data

In order to study ionospheric changes associated with the 2 July 2019 total solar eclipse, we utilized two dif-ferent types of geospace instruments: (1) a large network of GNSS receivers distributed over North and South America; (2) the Jicamarca Radio Observatory (JRO) incoherent scatter radar, located near the magnetic equator in Peru.

GNSS receivers offer a continuous high spatial and temporal resolution of ionospheric TEC. MIT Haystack Observatory processes more than 6,000 GNSS geodetic observables globally and provides access to this data through the Madrigal database system. Approximately 2,500 GNSS receivers located in North America and South America are used in the present study. The GNSS processing algorithms originally developed by Rideout and Coster (2006) and recently updated by Vierinen et al. (2016) are applied for the estimation of the GNSS-TEC. The TEC maps shown in this study utilize the vertical TEC converted from satellite-receiver pair (i.e., line of sight TEC) using the mapping function described by Rideout and Coster (2006).

JRO is an equatorial incoherent scatter radar (ISR). It is a VHF large aperture high-power ionospheric radar that operates at 49.92 MHz and is located at 11.57°S latitude and 76.52°W longitude (~2° geomagnetic latitude). JRO observations are mainly used here to study the equatorial ionosphere. We use the vertical plasma drift measurements from JRO collected during the 2019 solar eclipse. The technique of incoherent scatter as applied to the measurement of plasma drift at Jicamarca is discussed by Woodman and Hagfors (1969) and updated by Kudeki et al. (1999).

2.2. Method

The 2 July 2019 solar eclipse occurred during very low solar activity, as the solar flux (F10.7) varied from 68 to 70 SFU (1 SFU = 10^{-22} W/m^2/Hz) under generally quiet magnetic conditions with a Kp index of <3 unit throughout the 10 days considered for this study. We collected all data from 5 days before (27–30 June 2019; 1 July 2019) and 5 days after (03–07 July 2019) to represent the state of the ionosphere before and after the eclipse event. To provide information on eclipse perturbations from background, data on the eclipse day (2 July 2019) were normalized and subtracted from the 10-day mean of non-eclipse data and multiplied by 100 to obtain the TEC percentage deviation. The percentage deviation of TEC was also calculated for each non-eclipse day to capture the variability resulting from the eclipse forcing and separate it from variability due to other causes.

3. Results

Figure 1 shows the eclipse totality (100% obscuration) in thick black dotted curve and percentage partiality of the eclipse in black curves. The obscuration reaches ~70% near −15° of magnetic latitude in the southern crest of the EIA and ~ 30% at the magnetic equator. The geomagnetic latitudes are also represented in colored curves where the thick green curve represents the geomagnetic equator. Blue dots show locations of GNSS receiver stations.

Figure 2 shows the variation of TEC in 2-D maps during a day before (1 July 2019), the day of the eclipse (2 July 2019), and the day after the eclipse (3 July 2019) at 20:40 UTC, the time of total obscuration. The colored lines across the latitudes are the geomagnetic field lines, and the thick blue line is the geomagnetic equator. The black shaded circle indicates the spatial position of the eclipse at 20:40 UTC (the time the eclipse first made landfall). We observed a simultaneous increase and decrease in TEC around the crest of the EIA and around sub-EIA crest regions as indicated by the black and red dash ellipses in the middle panel, respectively. These enhancements and reductions were not observed on the days before and after the eclipse. To further investigate this TEC behavior, Figure 3a presents a keogram showing TEC around ±30° latitudes as a function of latitude and universal time. It is important to note that during all the dates examined in this study, the geomagnetic conditions were very quiet with Kp < 3 (except for 1 July with Kp = 3.3), the Dst less than −15 (except for 1 July with Dst = −20), and the average solar flux at 69 SFU. Readers should also note that all the GNSS-TEC keogram figures (i.e., TEC as a function of latitude and time) in this study were constructed for 65–75°W longitudes.

Figure 3a shows the 10-day TEC variation (at 65–75°W) during the control and the eclipse days. The green arrow indicates the eclipse day panel, the blue line indicates the onset of the eclipse, the first and second green lines indicate the start and end of partial obscuration as seen from land, and the red line represents the first landfall of the total solar eclipse. The black dotted ellipse indicates a large TEC enhancement at the EIA resulting from the eclipse forcing. From this keogram, we can easily identify the enhanced TEC at EIA crest as indicated by the black dotted ellipse, which is not visible on other days. This TEC enhancement started to form after the first appearance of the partial eclipse at 19.22 UT (first green line) and peaked
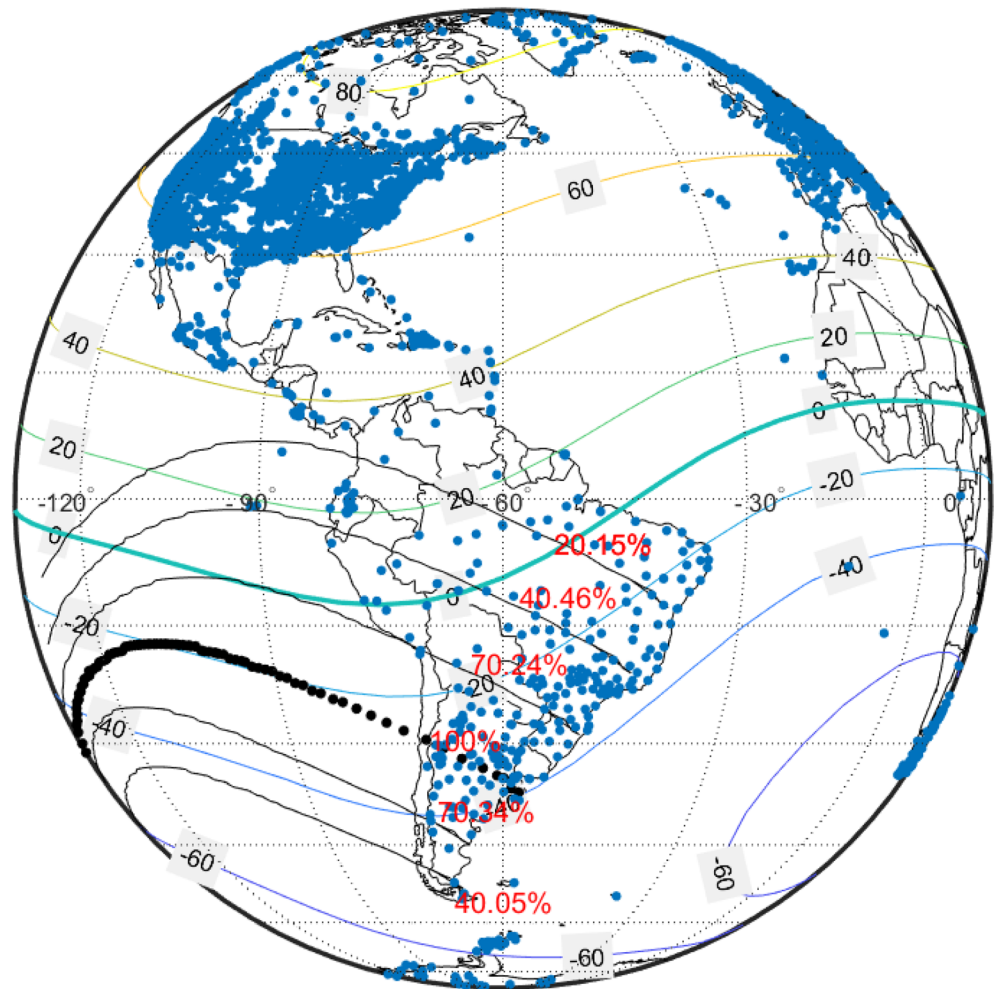
Figure 1. Eclipse totality (thick black curve), eclipse partiality (black lines in %), GNSS receiver stations (blue dotted cycles), the geomagnetic inclination along the latitudes (colored lines), magnetic equator (thick green curve).

at the first landfall (total obscuration) of the eclipse around 71°W at 20.44 UT. The enhanced TEC at the EIA continued even after the end of the partial obscuration (21.55 UT) and started to decrease about 10 min later (22.05 UT).

Figure 3b shows a clear TEC enhancement from ~19 UT to ~22 UT during the solar eclipse as referenced to the two control days, similar to Figure 3a. A reduction in TEC near ~18 UT is noted as well during eclipse day compared to 16 UT. The main reduction in TEC during the eclipse totality can also be clearly observed. Details of these features are indicated in Figure 4, and the mechanism is discussed in section 4.

For a more quantitative analysis and to highlight TEC enhancement and depletion at the EIA crest and along the eclipse totality (sub-EIA crest), we computed the average of TEC of 10 controlled days as a baseline value and subsequently subtracted each day from the average, plotting the results in Figure 4.

The top panel of Figure 4 represents the 10-day TEC mean, while the subsequent panels represent the TEC percentage deviation on selected control days as well as the eclipse day (indicated by the green arrow). Prior and post-eclipse days showed normal variation in TEC. However, on the eclipse day, a TEC bite-out was first observed around 16.30–18.30 UT just before the first partial obscuration was seen on land (at 71°W longitude). Afterwards, a simultaneous TEC enhancement and depletion was observed at the EIA crest region (85% obscuration) and along the part of the eclipse totality (100% obscuration), respectively. While the enhanced TEC at the EIA crest extended to a later time (possibly due to pre-reversal enhancement (PRE)
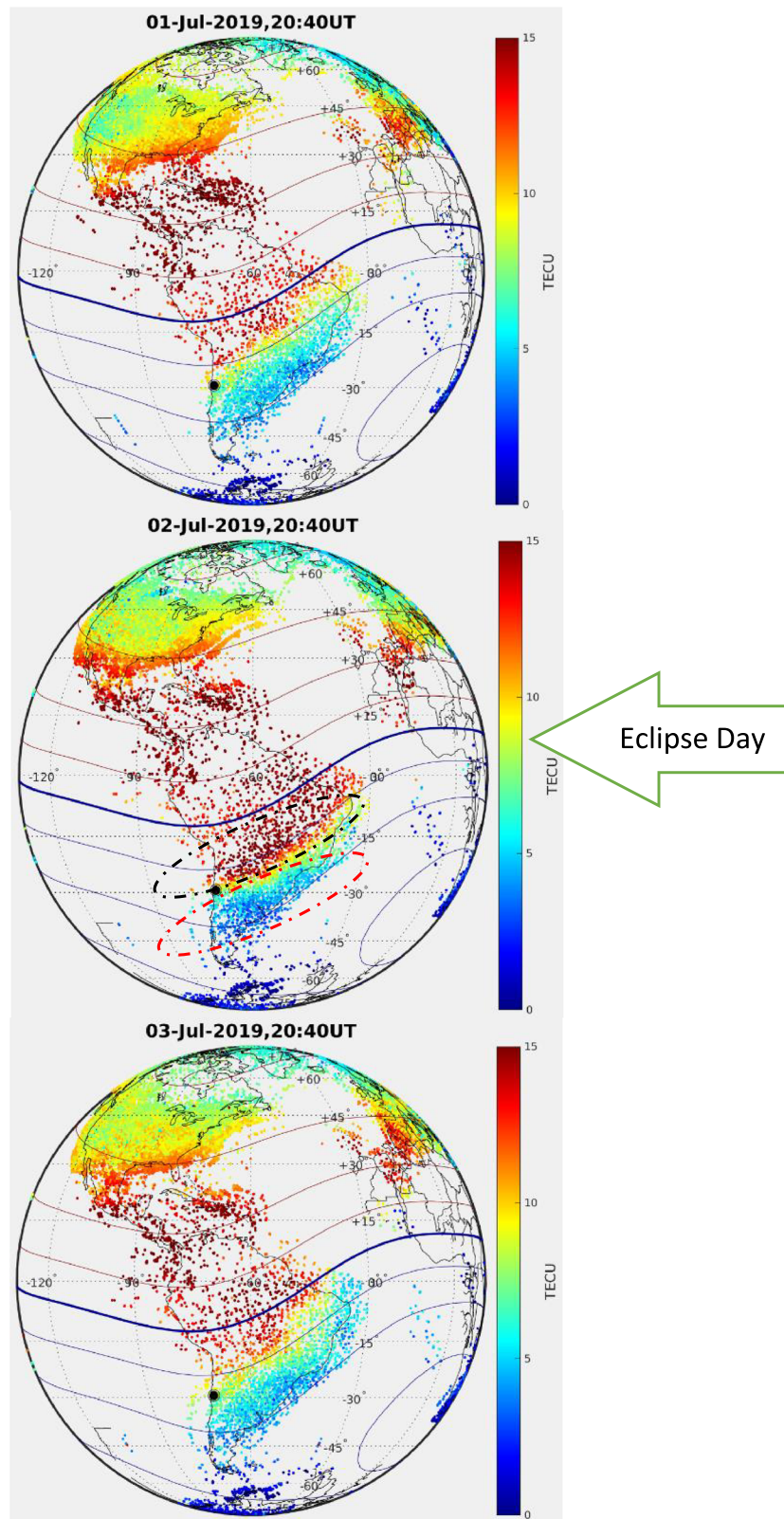
Figure 2. Variation of TEC on 1–3 July 2019. Non-eclipse reference days are represented by the top and bottom panels; the eclipse day is represented by the middle panel. The thick blue line represents the magnetic equator. The dashed black and red circles in the middle panel indicate the EIA and sub-EIA regions, respectively.
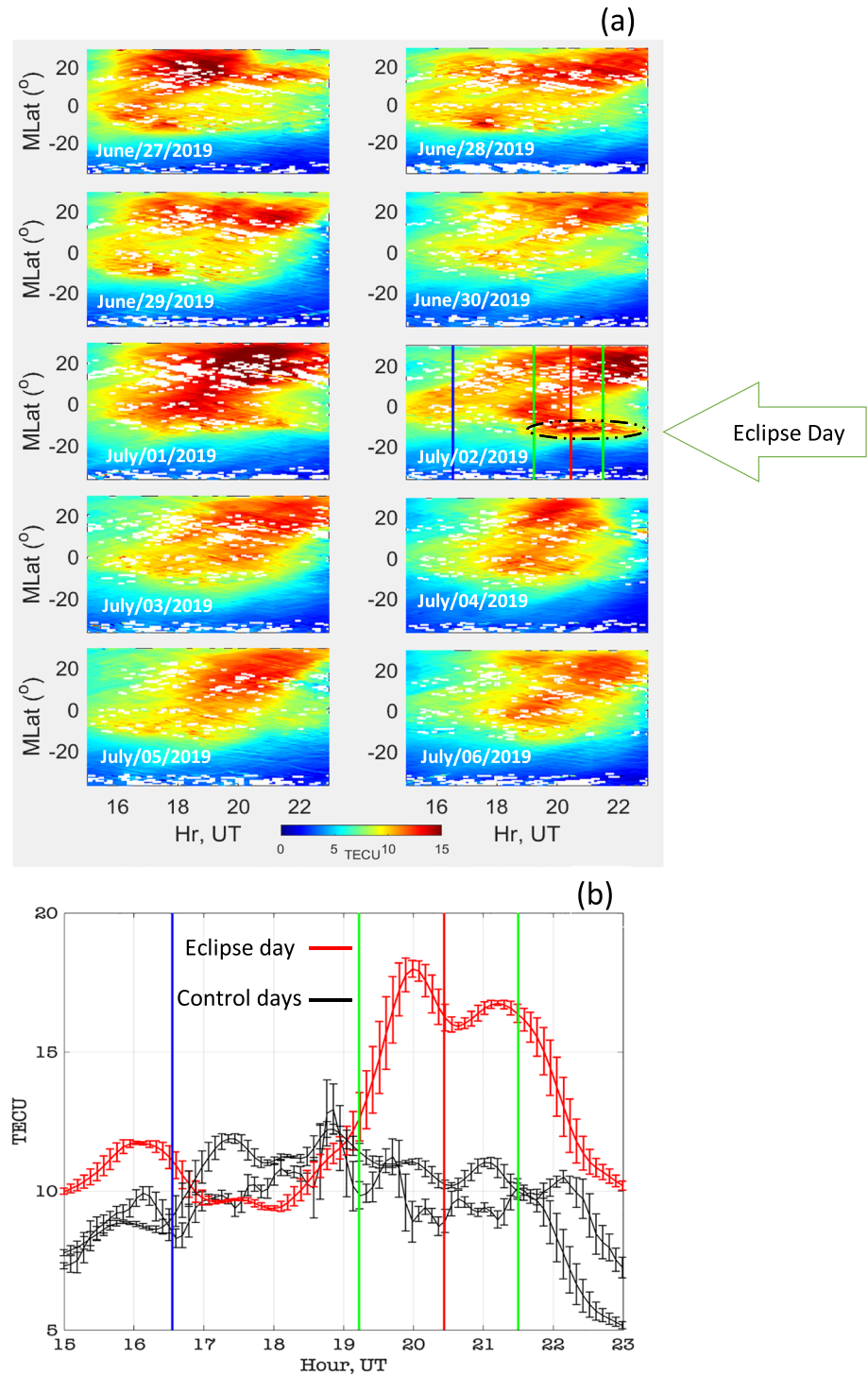
Figure 3. (a) The 10-day TEC variation (at 65–75°W) during the control and the eclipse periods. The green arrow indicates the eclipse day panel, the blue line indicates the onset of the eclipse, the first and second green lines indicate the start and end of partial obscuration as seen from land, and the red line represents the first landfall of the total solar eclipse. The black circle indicates the large TEC enhancement at the EIA resulting from the eclipse forcing. (b) 10.5°S latitudinal cut from (a) for eclipse day, 2 July (red curve), compared to control days 30 June and 3 July (black curves).

activity at the time), the depletion was short-lived. The TEC depletion lasted until the final eclipse obscuration at 21.55 UT. To further quantitatively understand the eclipse effect on the ionosphere, the percentage decrease and increase of TEC at the EIA crest and the sub-EIA crest were computed and are shown in Figure 5.

Figure 5a shows the percentage reduction and enhancement of TEC during the solar eclipse passage. In order to derive the percentage decrease and increase of the TEC changes around the EIA crest and sub-EIA crest, respectively, a cut around the EIA crest and sub-EIA crest regions was taken for the eclipse day, subtracted from the average of 10 non-eclipse days, and divided by 100. We found a minimum of 35% density reduction and maximum of 57% density enhancement at the EIA crest and sub-EIA crest, respectively, during the eclipse totality passage (further discussions given in section 4.1). On the other hand, Figure 5b shows signatures of the plasma fountain effect mechanism. The figure is derived by making a cut along 0 to −5°S of the magnetic equator on 4 selected control days (27–30 June) and the solar eclipse day (2 July). A substantial increase of plasma density occurred on eclipse day (green line) compared to other days (gray lines). Further details are given in section 4.2.

4. Discussion and Summary

4.1. Observed TEC Depletion and Density Bite-Out

Figure 4 (eclipse panel) provides a case study of how the ionosphere responds to the solar eclipse around the total obscuration region. Many previous solar eclipse studies show consistent depletion of ionization density during the total obscuration of the eclipse. For example, Ding et al. (2010) showed a 60% depletion of electron density at the F1 region over central China (26–36°N, 108–118°E) during eclipse total obscuration. Adeniyi et al. (2007) recorded a 68% ionization depletion in regions adjacent to the dip equator using ionogram-derived parameters such as hmF2 and foF2. Coster et al. (2017) also observed a strong depletion of TEC along the path of eclipse totality during the great American solar eclipse of August 2017. A depletion of about 50–60% was observed in the midlatitude region. For the 2 July 2019 solar eclipse that is the focus of the present study, we observed up to a 35% depletion of TEC in the sub-EIA region along the path of the eclipse totality between ~20.0 and 21.2 UT, as shown in Figure 4 (eclipse day). This depletion of electron density during the eclipse was caused by a drastic decrease in photoionization along the solar eclipse totality path within the Moon's shadow.

Another notable observation in Figure 4 is a decrease in the TEC near the southern crest of EIA, at ~ −10°MLAT, between ~16.30 and 19.00 UT, for example, soon after the onset of the solar eclipse but before the start of obscuration at this longitude. This decrease in ΔTEC (around this period) is known as the noontime bite-out. Past studies have shown that electron density bite-out typically occurs mostly around noontime at the magnetic equator. According to Rastogi et al. (1979) this bite-out is as a result of plasma uplift away from the magnetic equator by the fountain effect process, which consequently causes a sharp reduction of plasma at the equator known as noontime bite out. Rajaram (1977) pointed out that this noontime bite-out could also result from other mechanisms such as the complex interaction of daytime electrodynamic processes in the E and F regions or by a neutral wind distribution that transports plasma away from the equator. However, a recent study by Venkatesh et al. (2016) showed that electron density bite-out can also occur at low latitudes around the EIA crest region. They demonstrated that the bite-out at this region is driven by the downward gravity related force that moves topside ionization to lower altitudes (where recombination rate is high) while still maintaining minimum F-peak height. In our case, movement of plasma to low altitude would cause reduction in the plasma density due to higher recombination rates, causing a bite-out of electron density at the EIA crest.

The bite-out observed in this study was adjacent to the EIA crest and occurred around 16.30–18.45 UT (11.30–13.45 LT), in a manner similar to that of Venkatesh et al. (2016). However, as shown in Figure 4, among the 10 days of ΔTEC observation, only the eclipse day showed a noontime bite-out. Therefore, we suggest that the eclipse event on this day likely contributed to the formation of an electron density bite-out with mechanism examined by Venkatesh et al. (2016). We also note that the amplitude of the bite-out is quantitatively similar to the amplitude of the ΔTEC decrease observed at the sub-EIA crest during the totality of the solar eclipse event. The 2017 global simulation of Huba and Drob (2017) was focused on interhemispheric electrodynamic effects on electron content, and the study concluded that during eclipse
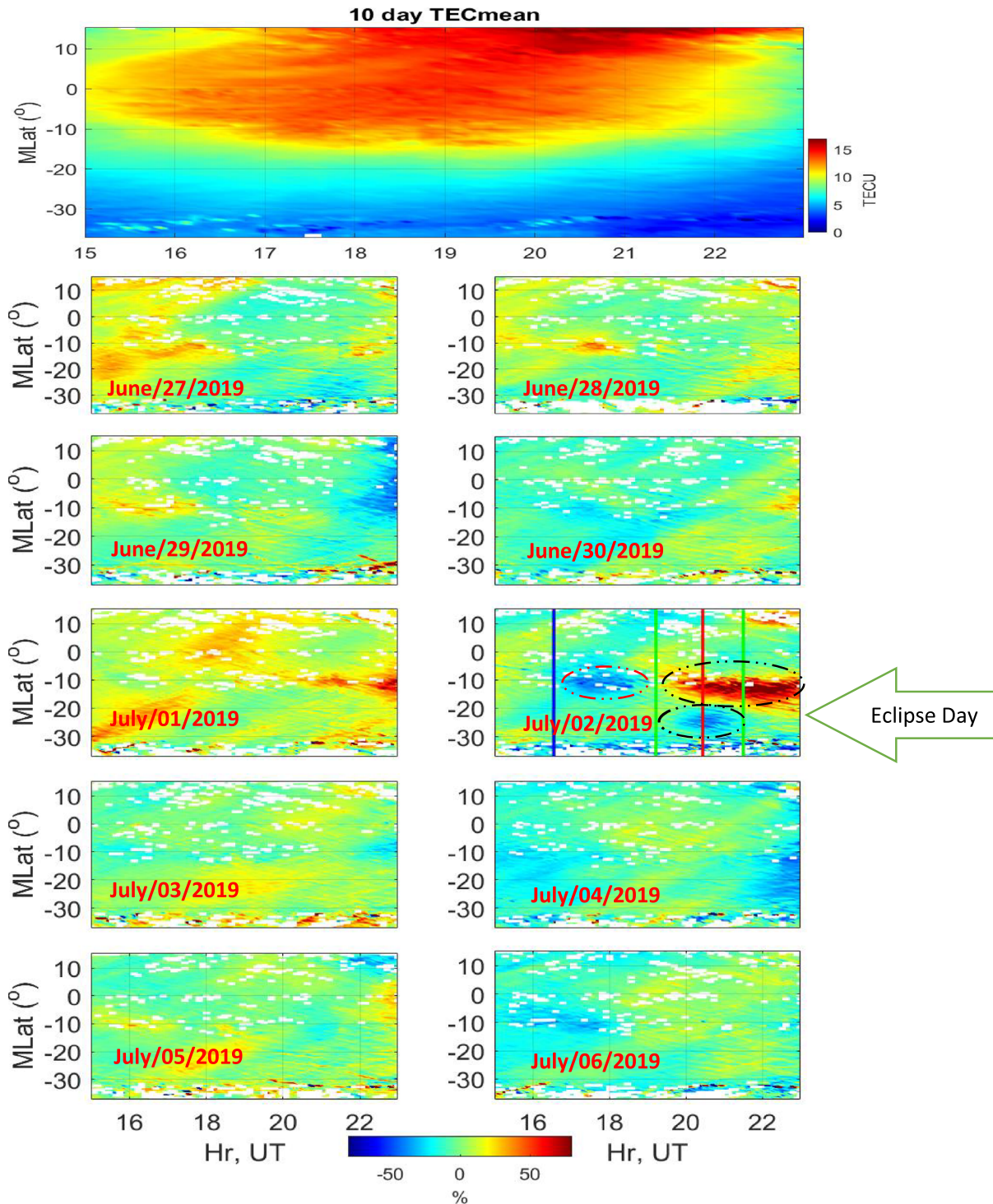
Figure 4. The 10-day TEC mean variation (at 65–75°W) during the non-eclipse period; subpanels represent TEC percentage deviation obtained from the 10-day mean. Blue line indicates the onset of the eclipse, the first and second green lines indicate the start and end of partial obscuration as seen from land, and the red line represents the first landfall of the total solar eclipse. The black circles indicate the large TEC enhancement at the EIA crest and depletion in sub-EIA crest resulting from the eclipse forcing. The red circle indicates a noticeable decrease around −10° after the onset of the eclipse.

conditions, continental size modification in electron density and conductance can modify the global electric field. The observed decrease in TEC prior to the start of the local solar obscuration is indeed consistent with a modification of the global electric field due to the decrease in the conductance that occurred along the path
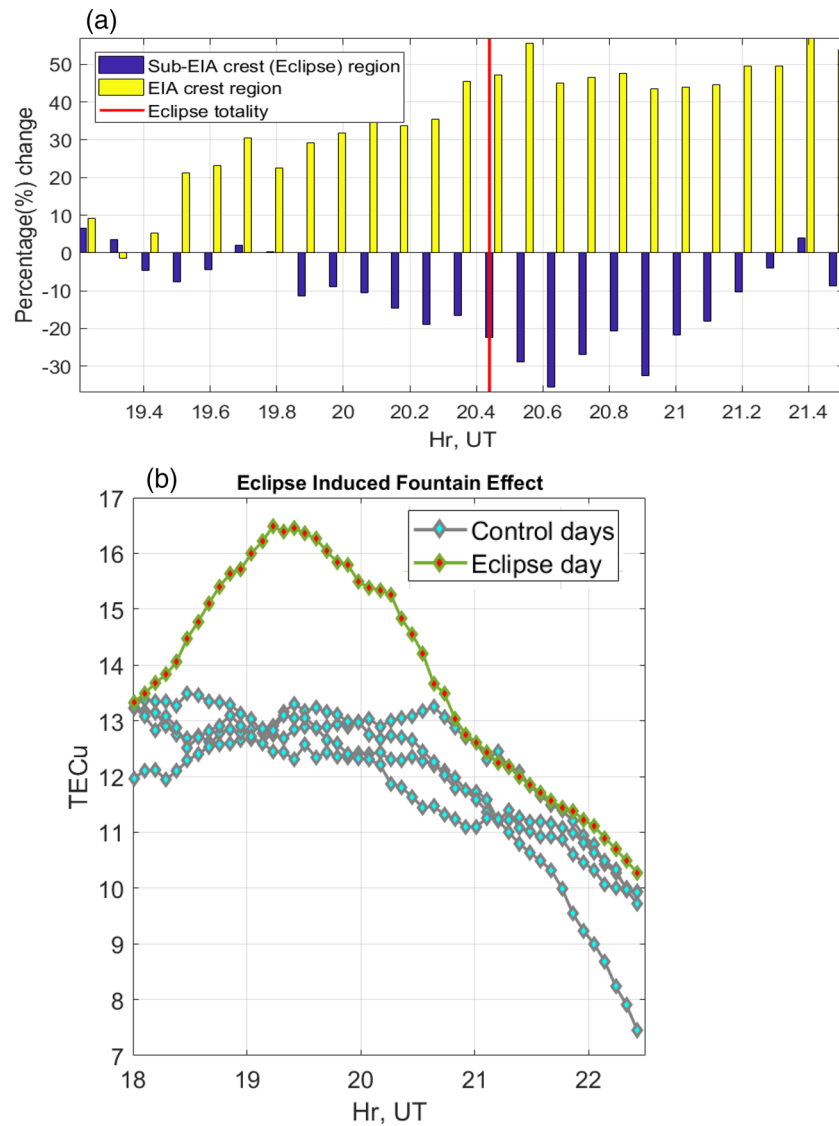
Figure 5. (a) Percentage enhancement of the EIA TEC (top bars) and percentage suppression of the sub-EIA TEC (bottom bars) during eclipse passage, mostly over land. The vertical red line indicates the first landfall of the eclipse totality. (b) A cut of TEC at 0–5°S for control days (27–30 June) represented with cyan-dotted gray line and eclipse day (2 July) represented with red-dotted green lines.

of the solar eclipse earlier and to the west from 65–75°W. This solar eclipse effect further implies that besides localized eclipse-induced perturbations, the solar eclipse might also have a broader impact on the global ionosphere-thermosphere system. In particular, Dang et al. (2018) indicated that through wind perturbation and electrodynamic coupling, eclipse effects can be global. Their simulation study showed that large scale traveling atmospheric disturbances (LSTADs) induced by the solar eclipse can manifest on a global scale as long bands of positive and negative perturbation in both neutral temperature and meridional wind. Future simulation studies of the July 2019 event would be very useful to further examine electrodynamic consequences of this equatorial region eclipse and to elucidate the role of ionospheric and thermospheric preconditioning.

4.2. Observed Ionization Enhancement at the EIA Crest (85% Obscuration)

The most unusual observation during the solar eclipse of 2 July was an ionization enhancement adjacent to the eclipse totality at a point which experienced 85% obscuration at the EIA crest region, as seen in Figures 4
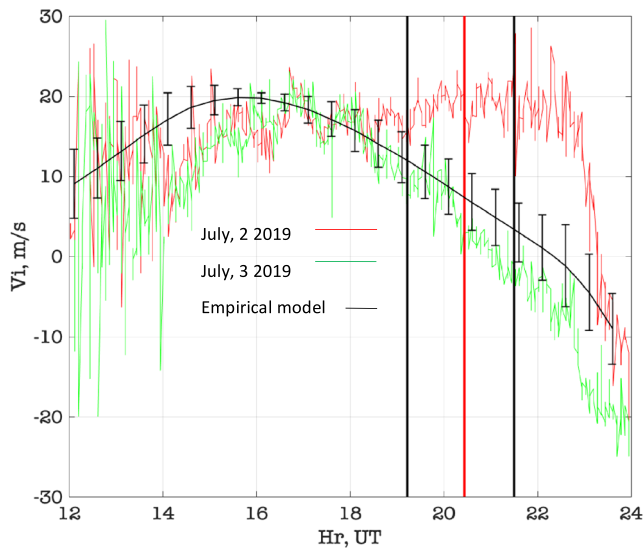
Figure 6. Observations of vertical plasma drift red at JRO (red for 2 July and green for 3 July) in comparison with vertical plasma drift climatology for low solar activity based on Scherliess and Fejer (1999) empirical model.

and 5a (top panel). As pointed out earlier in the introduction section, the plasma fountain effect plays an important role in the transportation of plasma from the equatorial region to form a peak (Appleton anomaly) at both sides of the magnetic equator round $\pm15°$ magnetic latitude. Sometimes, these two peaks of the EIA crest may vary in strength depending on seasonal interhemispheric wind (Jonah et al., 2015; Jones et al., 2018). Cheng et al. (1992) showed that the fountain effect is a dominant mechanism controlling the F2 peak density and height near the EIA crest region. In this study, besides the observed enhancement of ionization at the EIA crest during the eclipse totality (Figures 4 and 5a), we observed a substantial increase in electron density at the magnetic equator as shown in Figure 5b. This figure also provides insight into the behavior of the plasma fountain effect as related to the eclipse totality. It is interesting to note that ionization is largest during the eclipse day around the totality path as compared to any other day (in Figure 5b). Abdu (2005) pointed out that EIA and the equatorial electrojet (EEJ) associated with plasma fountain are driven by the same primary zonal electric field and that the force intensities are related. In particular, an intense (weak) plasma fountain can be associated with an enhanced (reduced) EIA. Our observations of 2019 eclipse effects are therefore consistent with a situation where more plasma is transported along the magnetic field lines through the enhanced plasma fountain to the EIA crest. This fact would give rise to the observed enhanced ionization at the EIA crest region as shown in Figures 2–4 (eclipse panels).

However, an important question remains: What could be responsible for the large ionization at the magnetic equator seen during the solar eclipse period relative to the controlled days? To investigate these electrodynamics, we used ISR measurements of vertical ion drifts at Jicamarca, 2°Mlat, −762°Glon (Sterling et al., 1972). The partial eclipse took place during 19.24–21.46 UT, with a maximum obscuration magnitude of the eclipse of 53.28% at 20.40 UT. Figure 6a shows the drift variability during the eclipse (red line) and day after the eclipse (green line). We observed vertical drift enhancement on the eclipse day (Figure 6 red curve) when compared with the day after the eclipse (Figure 6 green curve) and the expected mean value of equatorial vertical drift variation based on Scherliess and Fejer's (1999) empirical model (Figure 6 black curve with error bar). The vertical drift on 3 July (day after eclipse) is very consistent with this expected climatology showing a decreasing trend of the vertical drift toward evening hours without the characteristic dusk sector PRE. Remarkably, the vertical drift on 1 July appears to be also enhanced (figure not included because may be affected by other sources). We conclude that enhanced vertical drift on 1 July may likely be associated with either (a) fairly disturbed (Kp > 3) geomagnetic conditions or (b) enhanced dynamo action driven by lower atmospheric forcing, characterized as prominent 2-day oscillations of TEC day-to-day variations at low latitudes (Figure 3a) or both. The latter scenario is reinforced by the observation that TEC values near the northern EIA and partially the southern EIA were higher on 27 June, 29 June, and 1 July. Furthermore, Jicamarca drift day-to-day variation in the afternoon hours is indeed consistent with TEC, being higher on 1 July than on 3 July. In particular, if the 2-day observed drift oscillation pattern held, it implies the TEC EIA on 2 July, or the corresponding Jicamarca drift would be lower if the eclipse did not occur.

Additionally, the study by Chen et al. (2019) showed that eclipse-induced temperature and wind can play important roles in the TEC enhancement at the EIA crest observed before and after the eclipse's total obscuration. In the context of the present study, it is possible that atmospheric forcing due to neutral winds originating from the temperature (pressure) gradient induced by the solar eclipse may have caused an interaction with the magnetized conducting ionosphere that perturbed the U × B dynamo electric field. This enhanced electric field could map along the highly conducting magnetic field lines to equatorial F region heights to produce the observed enhanced plasma fountain that controls the plasma density distribution at the equatorial and low-latitude region as observed in most figures of this study. The enhanced vertical drifts measured at Jicamarca in this case would provide the needed driver to explain the enhanced fountain effect on electron density as seen in TEC.

We note that in addition to these potential mechanisms, increase in TEC at the EIA crest could also be related to other processes in the sub-EIA crest along the path of the solar eclipse described in section 4.1. Simulations of recent solar eclipses with different models indicate a formation of a decrease in thermospheric temperature with a center in the location of the shadow and a width of the order of tens of degrees in longitude (Cnossen et al., 2019; Wang et al., 2019; Wu et al., 2018). A resulting pressure gradient subsequently leads to localized disturbances in horizontal neutral winds directed toward the center of the pressure "hole" created by the eclipse along the sub-EIA crest region (see Figure 1). This geometry implies that the disturbance winds close to the EIA crest are directed mostly southward and eastward and contribute to the increase in electron density at the EIA crest. Determining the quantitative role of this physical pathway on eclipse ionospheric response can be further investigated in future works.

5. Summary

We presented here a study investigating ionospheric responses to the total solar eclipse of 2 July 2019 over the South American sector. Observations for this research are obtained from GNSS receivers and IS radar (Jicamarca). We found a simultaneous 35% decrease and a 57% increase in TEC in the sub-EIA crest and around the EIA crest, respectively, occurring during eclipse totality at sub-EIA latitudes. Although a reduction in TEC is common during eclipse periods, a long-lasting increase of ionization around the geomagnetic equator and EIA crest region is unusual and was clearly observed during eclipse totality passage. Analysis suggests that enhanced plasma fountain effects (at the magnetic equator) resulting from eclipse induced vertical drift and U × B dynamo electric field acted as the driving force of observed significant TEC enhancement at the EIA crest. Finally, we have presented unique observations of a noontime TEC bite-out prior to the start of the local partial eclipse. Additional future observations and simulations of this noontime TEC bite-out during similar events are needed to more firmly explore its association with the solar eclipse.

Data Availability Statement

Data for TEC processing are provided from the following organizations: UNAVCO, Scripps Orbit and Permanent Array Center, Institut Geographique National, France, International GNSS Service, The Crustal Dynamics Data Information System (CDDIS), National Geodetic Survey, Instituto Brasileiro de Geografia e Estatística, RAMSAC CORS of Instituto Geográfico Nacional de la República Argentina, Arecibo Observatory, Low-Latitude Ionospheric Sensor Network (LISN), Topcon Positioning Systems, Inc., Canadian High Arctic Ionospheric Network, Centro di Ricerche Sismologiche, Système d'Observation du Niveau des Eaux Littorales (SONEL), RENAG: REseau NAtional GPS permanent, GeoNet—the official source of geological hazard information for New Zealand, GNSS Reference Networks, Finnish Meteorological Institute, and SWEPOS, Sweden. Access to these data is provided by madrigal network via website (http://cedar.openmadrigal.org/).

References

Abdu, M. A. (2005). Equatorial ionosphere–thermosphere system: Electrodynamics and irregularities. *Advances in Space Research*, *35*(5), 771–787. https://doi.org/10.1016/j.asr.2005.03.150

Adeniyi, J. O., Radicella, S. M., Adimula, I. A., Willoughby, A. A., Oladipo, O. A., & Olawepo, O. (2007). Signature of the 29 March 2006 eclipse on the ionosphere over an equatorial station. *Journal of Geophysical Research*, *112*, A06314. https://doi.org/10.1029/2006JA012197

Chen, C. H., Lin, C. C., & Matsuo, T. (2019). Ionospheric responses to the 21 August 2017 solar eclipse by using data assimilation approach. *Earth and Planetary Science*, *6*(1), 13. https://doi.org/10.1186/s40645-019-0263-4

Cheng, K., Huang, Y. N., & Chen, S. W. (1992). Ionospheric effects of the solar eclipse of September 23, 1987, around the equatorial anomaly crest region. *Journal of Geophysical Research*, *97*, 103–111. https://doi.org/10.1029/91JA02409

Cnossen, I., Ridley, A. J., Goncharenko, L. P., & Harding, B. J. (2019). The response of the ionosphere-thermosphere system to the 21 August 2017 solar eclipse. *Journal of Geophysical Research: Space Physics*, *124*, 7341–7355. https://doi.org/10.1029/2018JA026402

Coster, A. J., Goncharenko, L., Zhang, S., Erickson, P. J., Rideout, W., & Vierinen, J. (2017). GNSS observations of ionospheric variations during the 21 August 2017 solar eclipse. *Geophysical Research Letters*, *44*, 12,041–12,048. https://doi.org/10.1002/2017GL075774

Dang, T., Lei, J., Wang, W., Zhang, B., Burns, A., Le, H., et al. (2018). Global responses of the coupled thermosphere and ionosphere system to the August 2017 great American solar eclipse. *Journal of Geophysical Research: Space Physics*, *123*, 7040–7050. https://doi.org/10.1029/2018JA025566

Ding, F., Wan, W., Ning, B., Liu, L., Le, H., Xu, G., et al. (2010). GPS TEC response to the 22 July 2009 total solar eclipse in East Asia. *Journal of Geophysical Research*, *115*, A07308. https://doi.org/10.1029/2009JA015113

Evans, J. V. (1965). On the behavior of f0F2 during solar eclipses. *Journal of Geophysical Research*, *70*(3), 733–738. https://doi.org/10.1029/JZ070i003p00733

Goncharenko, L. P., Erickson, P. J., Zhang, S.-R., Galkin, I., Coster, A. J., & Jonah, O. F. (2018). Ionospheric response to the solar eclipse of 21 August 2017 in Millstone Hill (42N) observations. *Geophysical Research Letters*, *45*, 4601–4609. https://doi.org/10.1029/2018GL077334

Huba, J. D., & Drob, D. (2017). SAMI3 prediction of the impact of the 21 August 2017 total solar eclipse on the ionosphere/plasmasphere system. *Geophysical Research Letters*, *44*, 5928–5935. https://doi.org/10.1002/2017GL073549

Jonah, O. F., de Paula, E. R., Muella, M. T. A. H., Dutra, S. L. G., Kherani, E. A., Negreti, P. M. S., & Otsuka, Y. (2015). TEC variation during high and low solar activities over South American sector. *Journal of Atmospheric and Solar - Terrestrial Physics*, *135*, 22–35. https://doi.org/10.1016/j.jastp.2015.10.005

Jones, M. Jr., Emmert, J. T., Drob, D. P., Picone, J. M., & Meier, R. R. (2018). Origins of the thermosphere-ionosphere semiannual oscillation formulating the "thermospheric spoon" mechanism. *Journal of Geophysical Research: Space Physics*, *123*, 931–954. https://doi.org/10.1002/2017JA024861

Kudeki, E., Bhattacharyya, S., & Woodman, R. F. (1999). A new approach in incoherent scatter F region E x B drift measurements at Jicamarca. *Journal OF Geophysical Research*, *104*(A12), 28,145-28,16. https://doi.org/10.1029/1998JA900110

Le, H., Liu, L., Yue, X., Wan, W., & Ning, B. (2009). Latitudinal dependence of the ionospheric response to solar eclipses. *Journal of Geophysical Research*, *114*, A07308. https://doi.org/10.1029/2009JA014072

Lin, C. Y., Deng, Y., & Ridley, A. (2018). Atmospheric gravity waves in the ionosphere and thermosphere during the 2017 solar eclipse. *Geophysical Research Letters*, *45*, 5246–5252. https://doi.org/10.1029/2018GL077388

Rajaram, G. (1977). Structure of the equatorial F region, top side and bottom side—A review. *Journal of Atmospheric and Terrestrial Physics*, *39*, 1125–1144. https://doi.org/10.1016/0021-9169(77)90021-6

Rastogi, R. G., Sethia, G., Chandra, H., Deshpande, M. R., Davies, K., & Murthy, B. S. (1979). Total electron content and F-region electron density distribution near the magnetic equator in India. *Journal of Atmospheric and Terrestrial Physics*, *41*(6), 561–564. https://doi.org/10.1016/0021-9169(79)90053-9

Rideout, W., & Coster, A. (2006). Automated GPS processing for global total electron content data. *GPS Solutions*, *10*, 219–228. https://doi.org/10.1007/s10291-006-0029-5

Rishbeth, H. (1968). Solar eclipses and ionospheric theory. *Space Science Reviews*, *8*(4), 543–554.

Scherliess, L., & Fejer, B. G. (1999). Radar and satellite global equatorial F region vertical drift model. *Journal of Geophysical Research*, *104*(A4), 6829–6842. https://doi.org/10.1029/1999JA900025

Sterling, D. L., Hanson, W. B., & Woodman, R. F. (1972). Synthesis of data obtained at Jicamarca, Peru, during the September 11, 1969, eclipse. *Radio Science*, *7*(2), 279–289. https://doi.org/10.1029/RS007i002p00279

Tomás, A. T., Lühr, H., Förster, M., Rentz, S., & Rother, M. (2007). Observations of the low latitude solar eclipse on 8 April 2005 by CHAMP. *Journal of Geophysical Research*, *112*, A06303. https://doi.org/10.1029/2006JA012168

Venkatesh, K., Fagundes, P. R., de Abreu, A., & Pillat, V. G. (2016). Unusual noon-time bite-outs in the ionospherec electron density around the anomaly crest locations over the Indian and Brazilian sectors during quiet conditions—A case study. *Journal of Atmospheric and Solar-Terrestrial Physics*, September, *147*, 126–137. https://doi.org/10.1016/j.jastp.2016.07.016

Vierinen, J., Coster, A. J., Rideout, W. C., Erickson, P. J., & Norberg, J. (2016). Statistical framework for estimating GNSS bias. *Atmospheric Measurement Techniques*, *9*, 1303–1312. https://doi.org/10.5194/amt-9-1303-2016

Wang, W., Dang, T., Lei, J., Zhang, S., Zhang, B., & Burns, A. (2019). Physical processes driving the response of the F2 region ionosphere to the 21 August 2017 solar eclipse at Millstone Hill. *Journal of Geophysical Research: Space Physics*, *124*, 2978–2991. https://doi.org/10.1029/2018JA025479

Wang, X., Berthelier, J. J., & Lebreton, J. P. (2010). Ionosphere variations at 700 km altitude observed by the DEMETER satellite during the 29 March 2006 solar eclipse. *Journal of Geophysical Research*, *115*, A11312. https://doi.org/10.1029/2010JA015497

Woodman, R. F., & Hagfors, T. (1969). Methods for the measurement of vertical ionospheric motions near the magnetic equator by incoherent scattering. *Journal OF Geophysical Research: Space Physics*, *74*(5), 1205–1212. https://doi.org/10.1029/JA074i005p01205

Wu, C., Ridley, A. J., Goncharenko, L., & Chen, G. (2018). GITM-data comparisons of the depletion and enhancement during the 2017 solar eclipse. *Geophysical Research Letters*, *45*, 3319–3327. https://doi.org/10.1002/2018GL077409

Zhang, S., Erickson, P. J., Goncharenko, L., Coster, A. J., Rideout, W., & Vierinen, J. (2017). Ionospheric bow waves and perturbations induced by the 21 august 2017 solar eclipse. *Geophysical Research Letters*, *44*, 12,067–12,073. https://doi.org/10.1002/2017GL076054